ESI: Tuning electrocatalytic water oxidation by MnO$_x$ through the incorporation of abundant metal cations

Jens Melder[*,‡,a], Stefan Mebs[*,b], Florian Lessing[a], Holger Dau[b], Philipp Kurz[a]

[a]Institut für Anorganische und Analytische Chemie and Freiburger Materialforschungszentrum (FMF), Albert-Ludwigs-Universität Freiburg, Albertstraße 21, 79104 Freiburg (Germany)
[b]Fachbereich Physik, Freie Universität Berlin, Arnimallee 14, 14195 Berlin, Germany
[‡]Present address: German Aerospace Center, Institute of Combustion Technology, Pfaffenwaldring 38-40, 70569 Stuttgart (Germany)

1 Materials and methods

All reagents and solvents were purchased from commercial sources and, unless otherwise stated, used without further purification. For the preparation of the potassium phosphate buffer, the potassium hydroxide solution and the stock solutions for fAAS measurements ultra-pure water (ELGA PURE-LAB flex) was used. All other experiments were carried out in deionised water.

ATR-FT-IR-spectroscopy IR spectra of the M_yMnO_x/CFP -electrodes before and after electro-chemical long-term treatment were carried out with a Nicolet 13 iS10 FT-IR spectrometer (Thermo Fisher Scientific) equipped with a diamond ATR-unit.

Grazing incidence powder X-ray diffractometry (GI-XRD) GI-XRD patterns of M_yMnO_x/CFP-electrodes were recorded in reflection geometry with a Seifert 3003 TT diffractometer and Cu-Kα-radiation. The electrodes were therefore mounted on a Plexiglas holder.

Scanning electron microscopy and energy dispersive X-ray analysis (SEM and EDX) SEM was performed using a FEG-SEM SU8220 (Hitachi) equipped with a secondary electron in-lens detector and four Bruker silicon drift detectors (sdd) for EDX analysis. The images were taken in a distance of approximately 2.5 mm with an acceleration voltage of 2.5 kV. EDX analyses were performed at a distance of 15 mm and acceleration voltages of 15 kV.

Flame atomic absorption spectroscopy (fAAS) Concentrations of manganese, potassium, cobalt, iron, calcium and nickel ions were determined with a fAAS novAA350 (Analytik Jena). A solution of HNO3 (1 %, w/w) served as diluent and the fAAS was calibrated with K-, Mn(II)-, Co(II)-, Ca(II)-, Ni(II)- and Fe(II)-nitrate standard solutions (Roth). Prior to analysis, the M_yMnO_x/CFP electrodes were treated with 0.1 mL of a 1 : 10-mixture of concentrated HNO_3 and 30 % H_2O_2, which completely dissolved the oxide from the carbon support and converted all metal ions to their soluble M^{2+} form. The solutions were then diluted to 25 mL. Electrolytes were directly measured without any further dilution.

XANES and EXAFS were conducted at the KMC3 beamline of the BESSY synchrotron operated at the Helmholtz-Zentrum Berlin (HZB). Data collection was performed at 20 K in a liquid-helium cryostat in fluorescence detection mode using a 13 element ultra-low energy resolving Ge detector (Canberra). Over 20 spectra were averaged for each compound in order to improve the signal-to-noise ratio. Averaged spectra were background-corrected and normalized using in-house software. Subsequently, unfiltered k_3-weighted spectra and phase functions from FEFF8.5[1] were used for least-squares curve-fitting of the EXAFS with in-house software and for calculation of Fourier-transforms representing k-values between 2 and 14 Å^{-1}. The fits were performed using the Levenberg-Marquardt method with numerical derivatives. The error ranges of the fit parameters were approximated from the covariance matrix of the fit. Data were multiplied by a fractional cosine window (10 % at low and high k-side). The amplitude reduction factor S_0^2 was 0.7 for Mn, 0.75 for Fe, 0.8 for Co, and 0.9 for Ni.

Preparation of K-phosphate buffer solutions Potassium phosphate buffer solutions with different pH were prepared from concentrated phosphoric acid (85 %, ACS quality) by dilution with

ultra-pure water. The pH was adjusted by adding KOH pellets (ACS quality). All pH measurements were carried out with an inolab ids 9310 pH-meter from WTW equipped with a SenTix980 pH electrode.

Electrochemistry

To evaluate the electrocatalytic behavior of the M_yMnO_x/CFP-electrodes a multi-step protocol was used. EIS measurements for the determination of the uncompensated resistance were performed at the open circuit potential (OCP) by applying an AC voltage with an amplitude of 10 mV_{RMS} in a frequency range of 100 kHz to 10 Hz. For the determination of Tafel-plots a staircase type chronoamperometry program in which the potential of the working electrode was increased stepwise from 1.22 to 2.02 V vs. RHE was used. At each step the potential was held constant for 300 s (5 min). To calculate the Tafel-plots the average over the last 30 s of the current-density j at the end of each upward staircase was calculated. Cyclic voltammograms were recorded for the range of 0.92-2.02 V vs. RHE with a scan rate of 20 mV s^{-1}.

EIS data were analyzed with the ZView software package from Scribner Associates. For the simulation of the EIS data, an equivalent circuit based on a simple Randless cell was used. The double-layer capacitance was modeled as a constant phase element owing to the porous structure of the electrode.
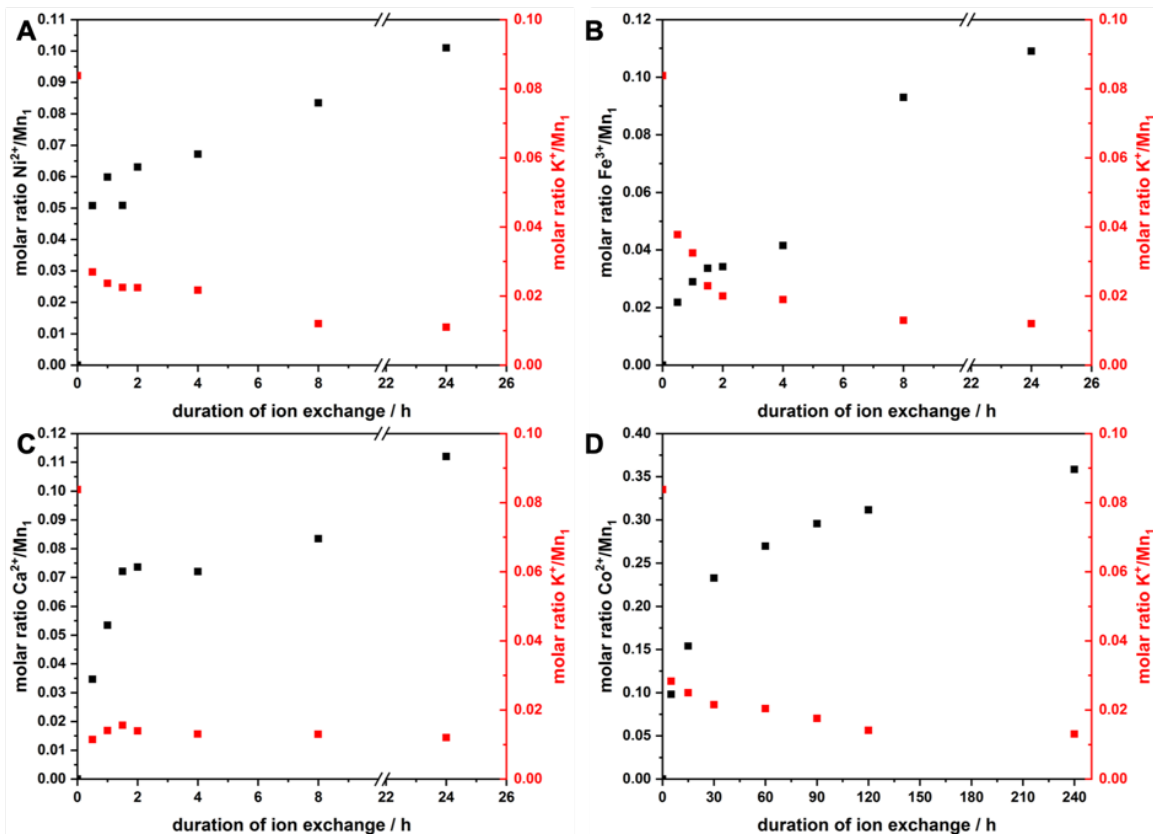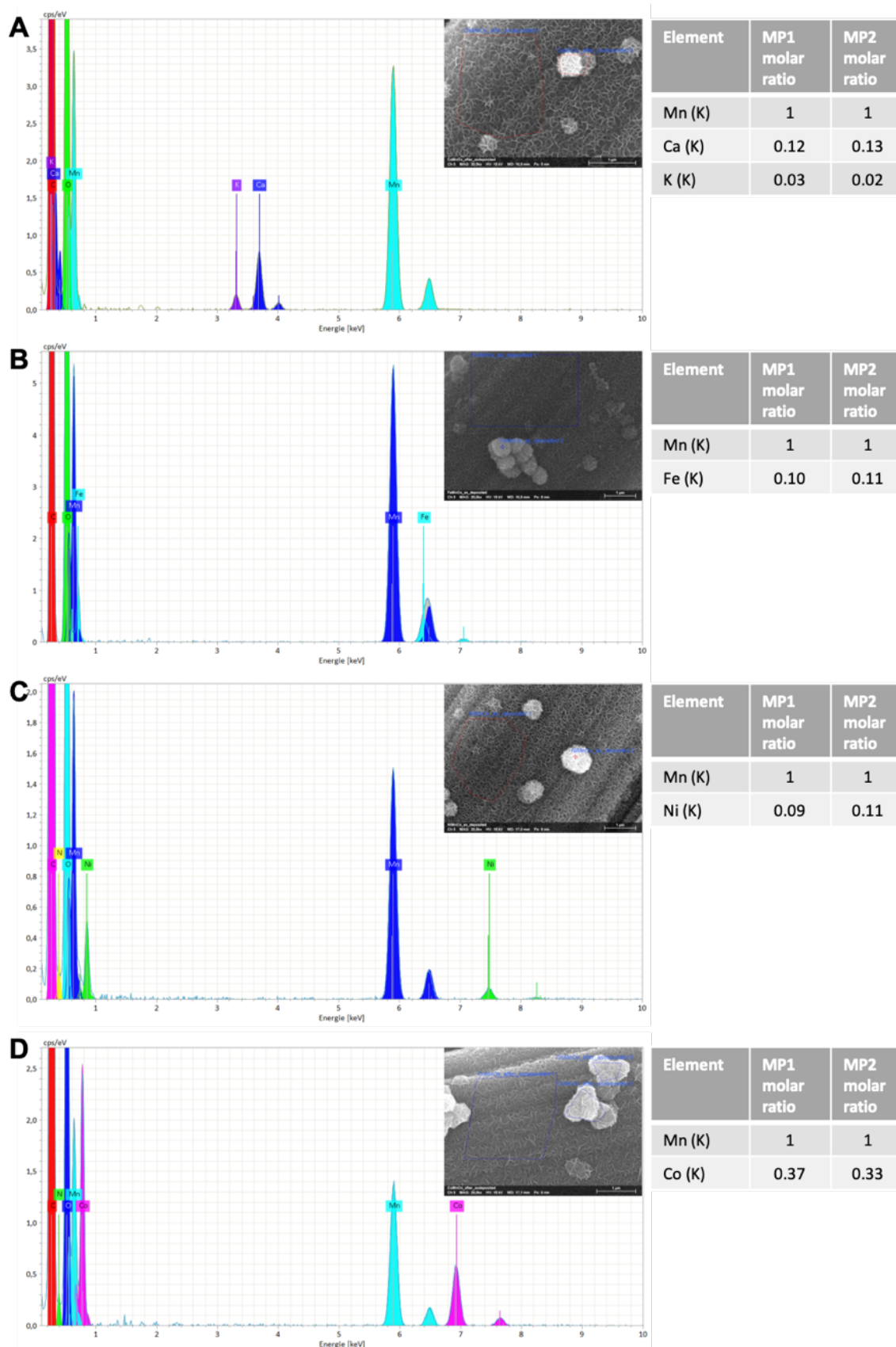
2 Additional figures and tables


Fig. S 1: amount of cations exchanged over time and in proportion to the amount of manganese ions for M_yMnO_x/CFP-electrodes. The molar metal ratios were determined by fAAS after dissolution of the catalyst from the CFP support. All shown data points are the average of two individual measurements.

Element	MP1 molar ratio	MP2 molar ratio
Mn (K)	1	1
Ca (K)	0.12	0.13
K (K)	0.03	0.02

Element	MP1 molar ratio	MP2 molar ratio
Mn (K)	1	1
Fe (K)	0.10	0.11

Element	MP1 molar ratio	MP2 molar ratio
Mn (K)	1	1
Ni (K)	0.09	0.11

Element	MP1 molar ratio	MP2 molar ratio
Mn (K)	1	1
Co (K)	0.37	0.33

Fig. S 2: Typical EDX spectra of as-prepared $M_y MnO_x$/CFP-electrode (A: Ca, B: Fe, C: Ni, D: Co); the SEM micrograph shows the position where the EDX spectra were recorded; the table shows the molar ratios of M : Mn (M = Ca, Co, Ni, Fe, K). The signal of C originates from the catalyst support.
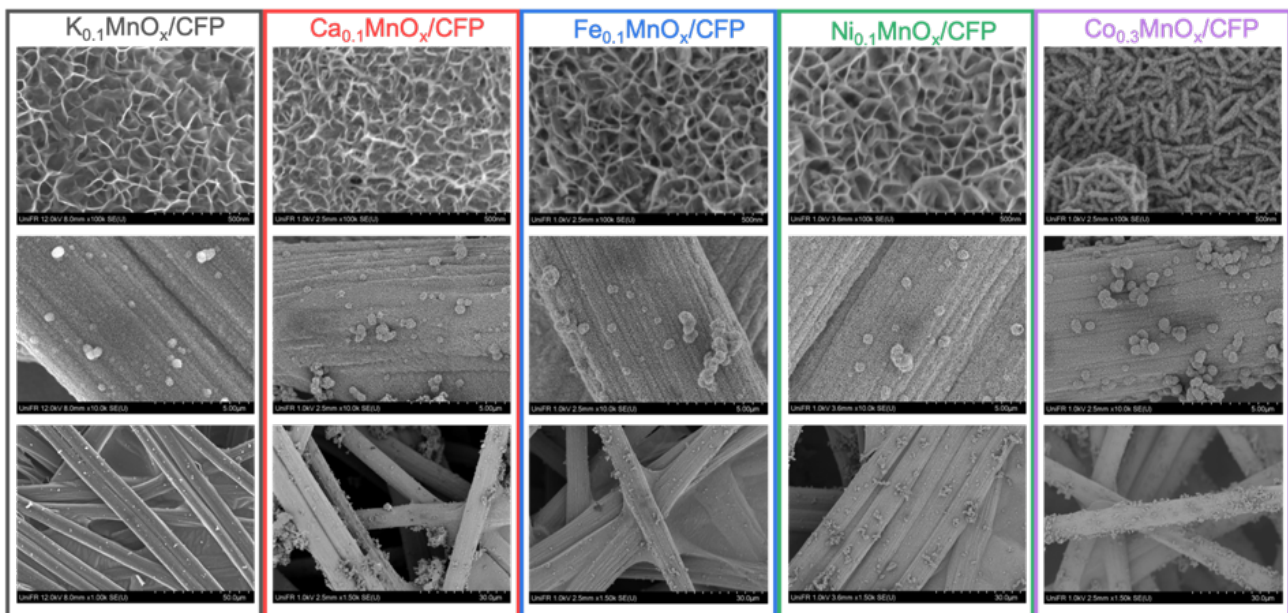
Fig. S 3: Additional SEM micrographs at different magnifications (top row: x100k; middle row: x10k; lower row: x1k) of the as prepared $M_y MnO_x$/CFP-electrodes.
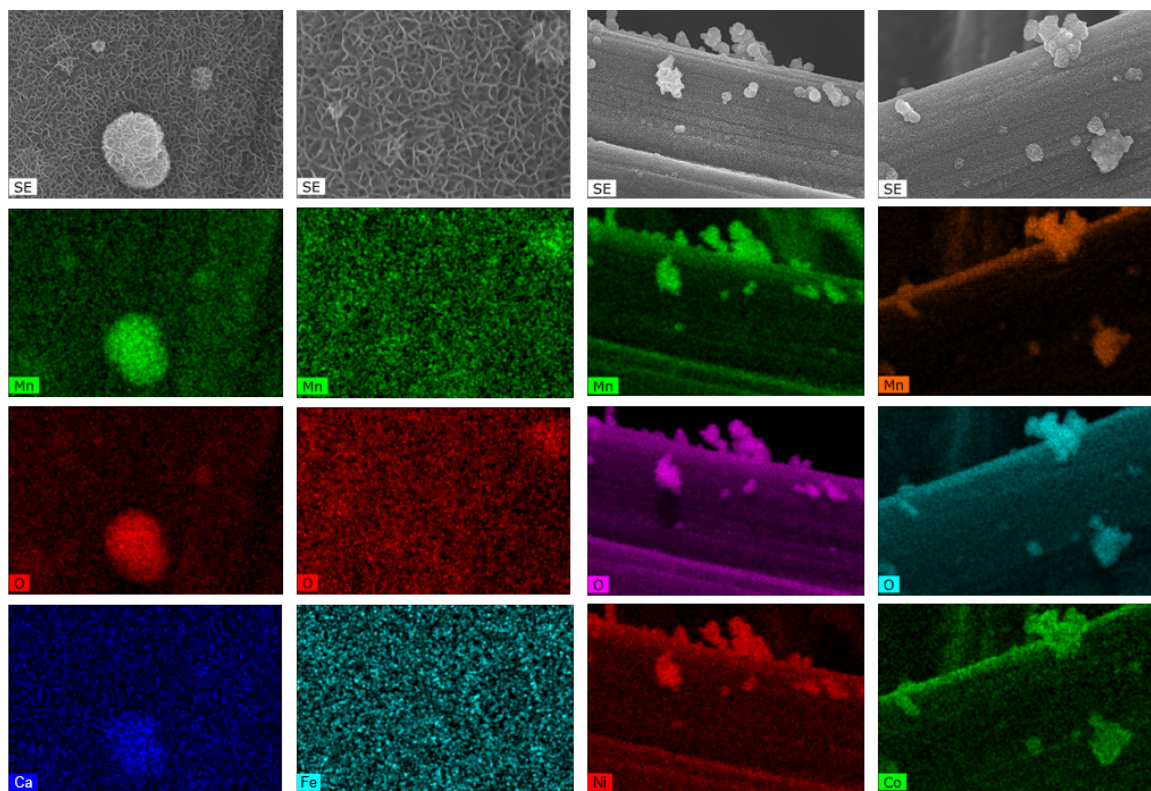
Fig. S 4: EDX elemental mapping of freshly prepared $Ca_{0.1}MnO_x$/CFP, $Fe_{0.1}MnO_x$/CFP, $Ni_{0.1}MnO_x$/CFP and $Co_{0.3}MnO_x$/CFP-electrodes.
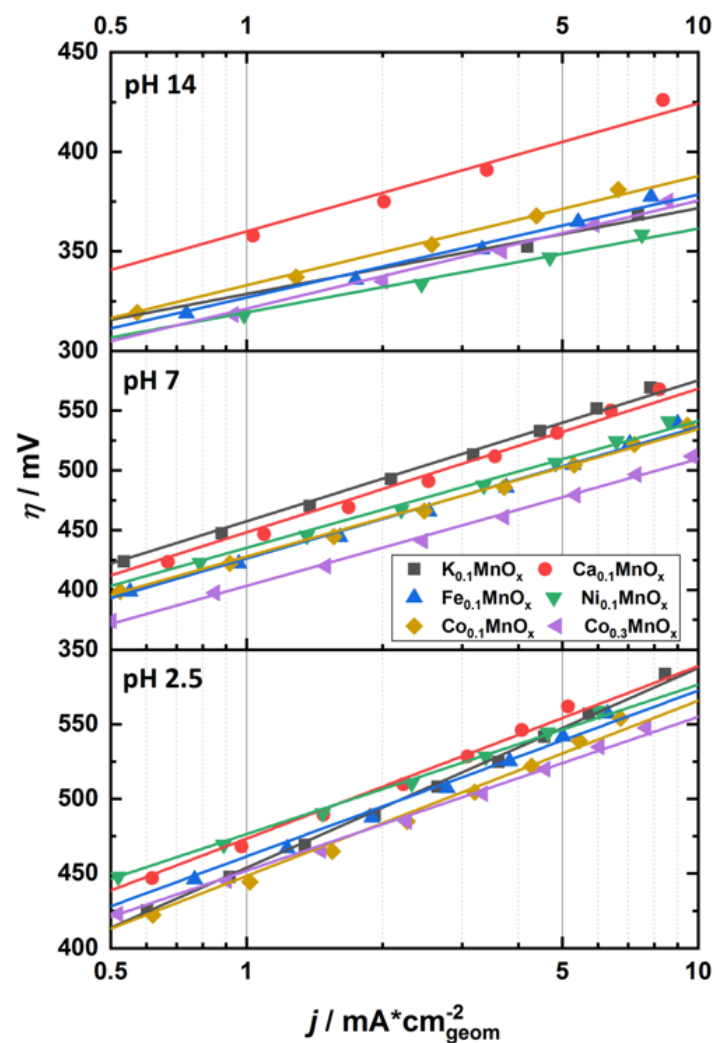
Fig. S 5: Tafel plots of M_yMnO_x/CFP-electrodes at different pH regimes and normalized to the geometric area; extracted from stepwise chronoamperometry measurements. All shown traces are the average of two individual measurements.
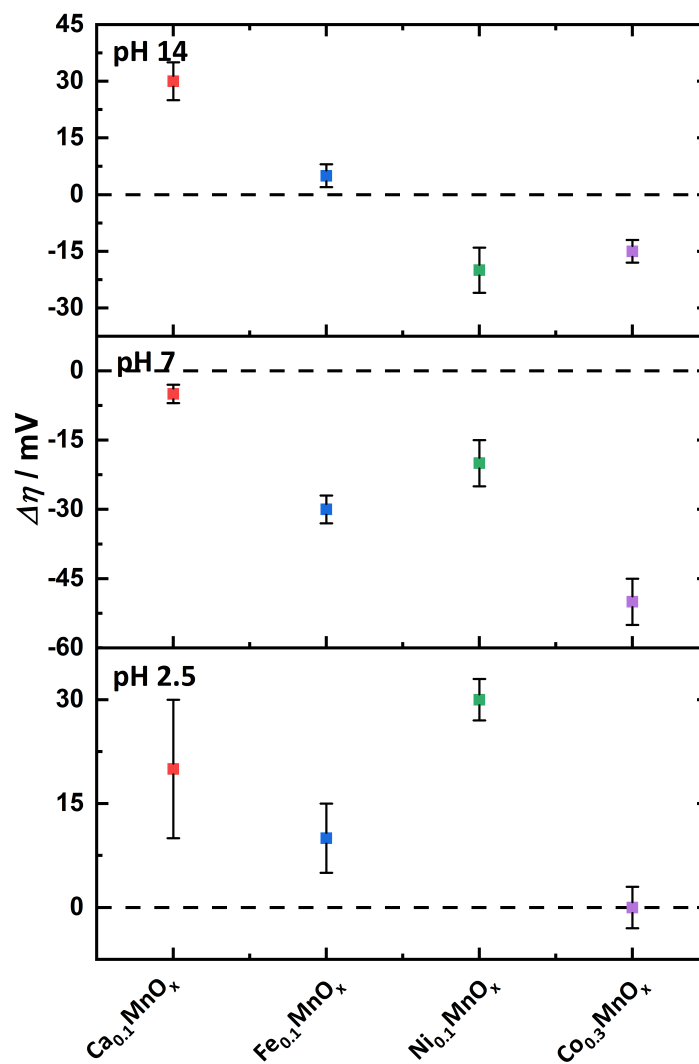
Fig. S 6: difference $\Delta\eta$ between the overpotential needed to reach a current density of 1 mA cm^{-2} by the mature electrode (K$_{0.1}$MnO$_x$/CFP) in comparison to the other tested M$_y$MnO$_x$/CFP-electrodes. All shown traces are the average of two individual measurements. The error bars represent one standard deviation.
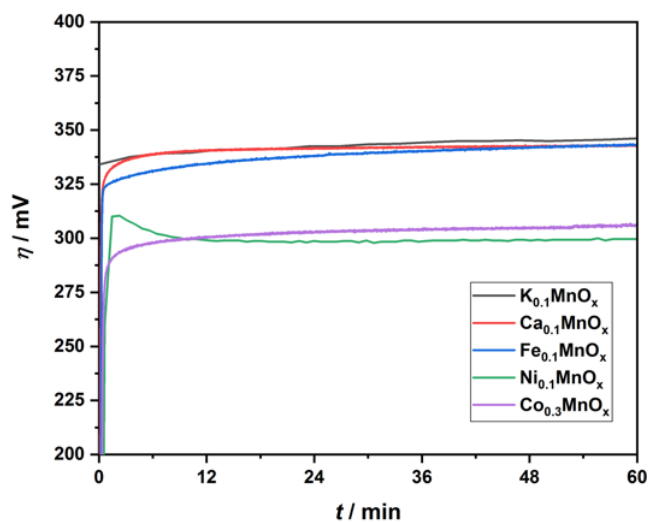
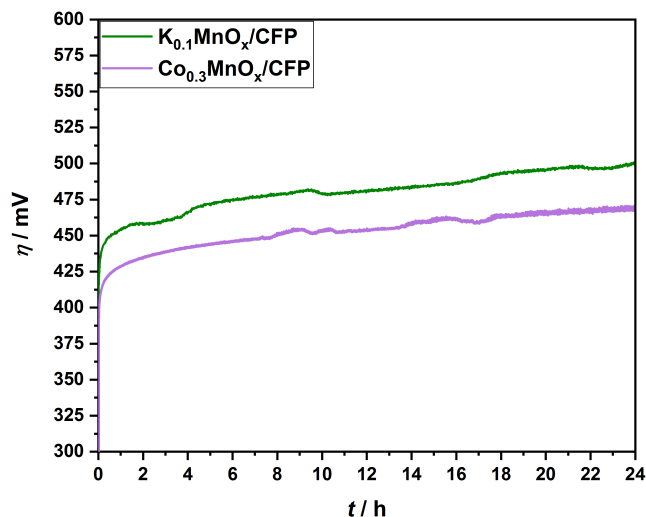**Fig. S 7:** First hour of the long-term electrolysis experiment at $j = 2$ mA cm^{-2} at pH 14.0. The complete 22 h are shown in Fig. **??**c of the main text. All shown traces are the average of two individual measurements.
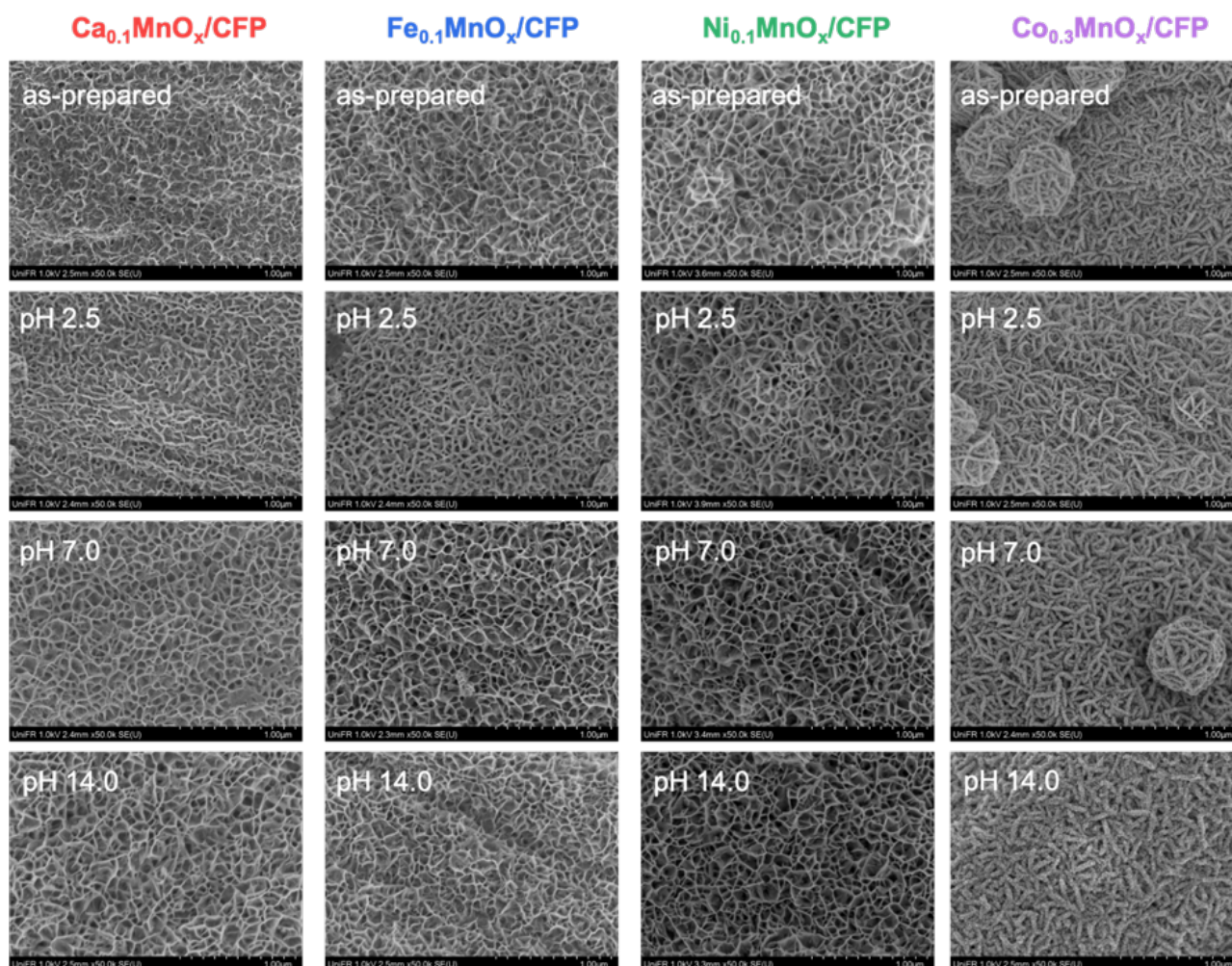
Fig. S 8: SEM micrographs of the $M_y MnO_x$/CFP-electrodes after electrochemical long-term operation at pH 2.5, 7.0 and 14.0.

Fig. S 9: Long-term stability of a $Co_{0.3}MnO_x$/CFP-electrode during constant application of $j = 2$ mA cm^{-2} in comparison to a $K_{0.1}MnO_x$/CFP-electrode exhibiting nearly the identical number of Mn-ions (n(Co + Mn)$_{AAS}$ = 3.9 μmol cm^{-2} vs. n(Mn)$_{AAS}$ = 4.0 μmol cm^{-2}. All shown traces are the average of two individual measurements.

at. %	pH 2.5	pH 7.0	pH 14.0
Mn	1	1	1
K	0.15	0.13	0.05
P	0.15	0.14	-
Ca	0.05	0.05	0.12
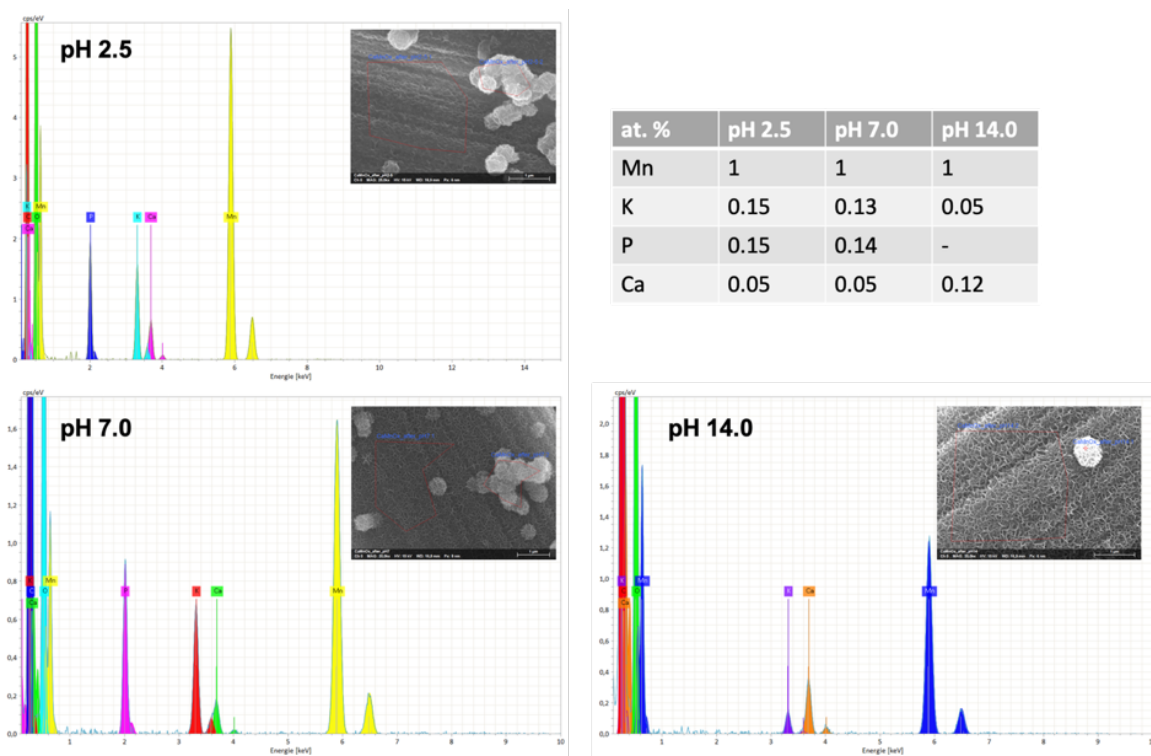
Fig. S 10: Typical EDX spectra of $Ca_{0.1}MnO_x$/CFP-electrodes after electrochemical long-term operation at pH 2.5, 7.0 and 14.0; the SEM micrograph shows the position where the EDX spectra were recorded; the table shows the molar ratios. The signal of C originates from the catalyst support.
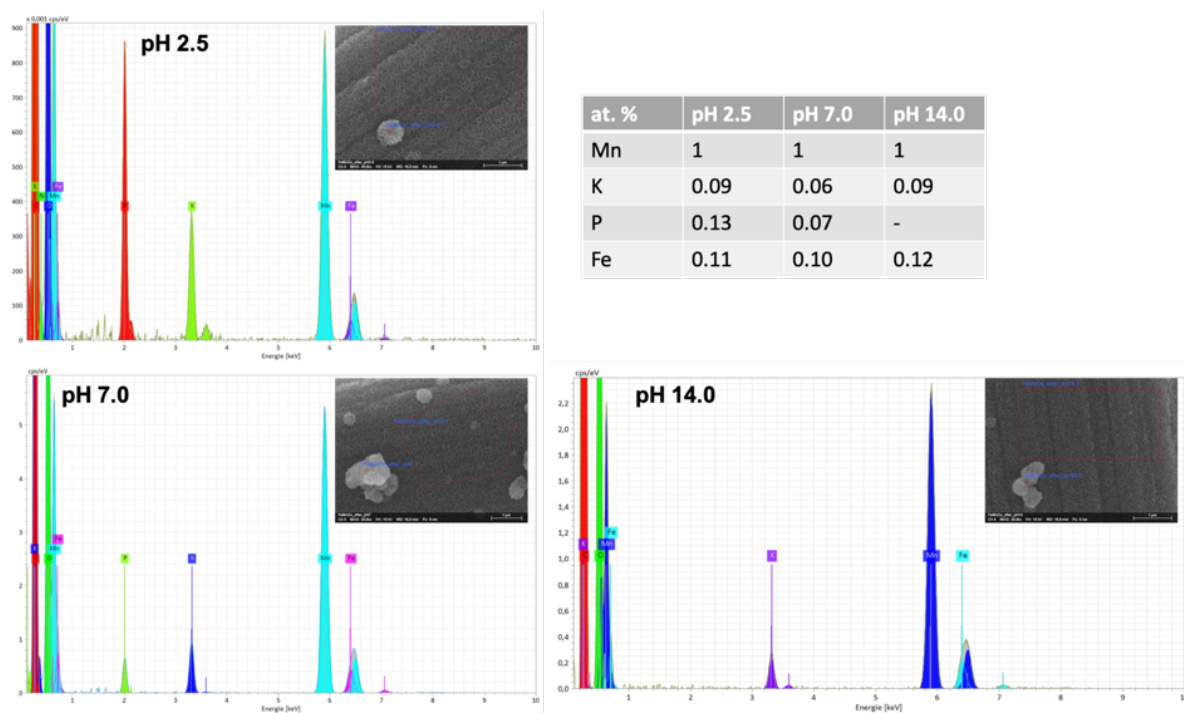
Fig. S 11: Typical EDX spectra of $Fe_{0.1}MnO_x$/CFP-electrodes after electrochemical long-term operation at pH 2.5, 7.0 and 14.0; the SEM micrograph shows the position where the EDX spectra were recorded; the table shows the molar ratios. The signal of C originates from the catalyst support.

at. %	pH 2.5	pH 7.0	pH 14.0
Mn	1	1	1
K	0.09	0.06	0.09
P	0.13	0.07	-
Fe	0.11	0.10	0.12
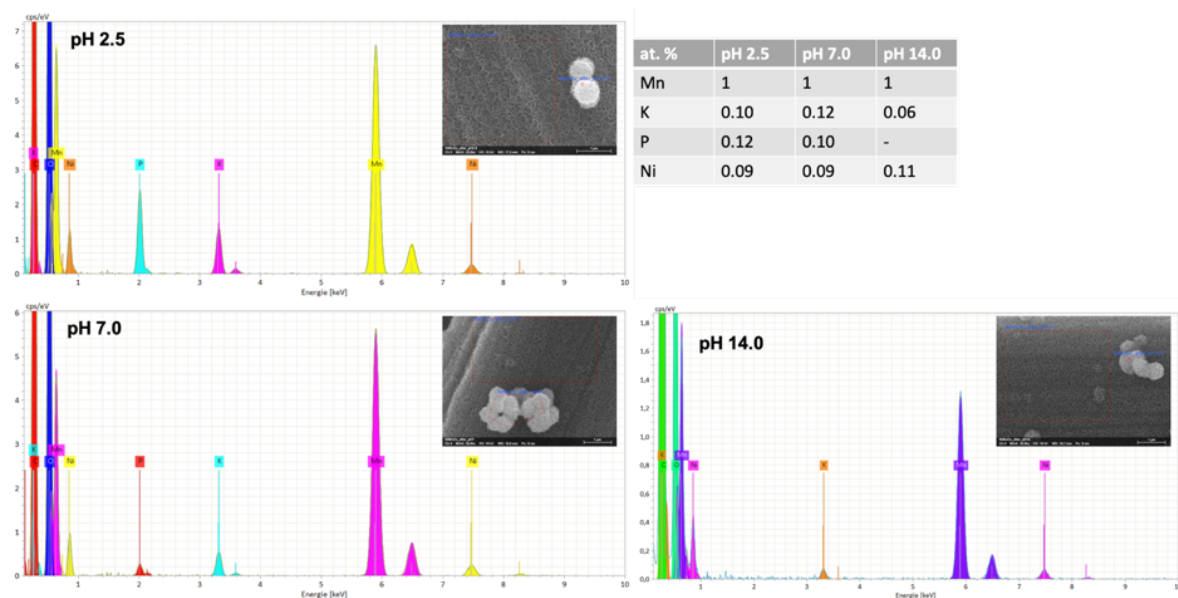
Fig. S 12: Typical EDX spectra of $Ni_{0.1}MnO_x$/CFP-electrodes after electrochemical long-term operation at pH 2.5, 7.0 and 14.0; the SEM micrograph shows the position where the EDX spectra were recorded; the table shows the molar ratios. The signal of C originates from the catalyst support.

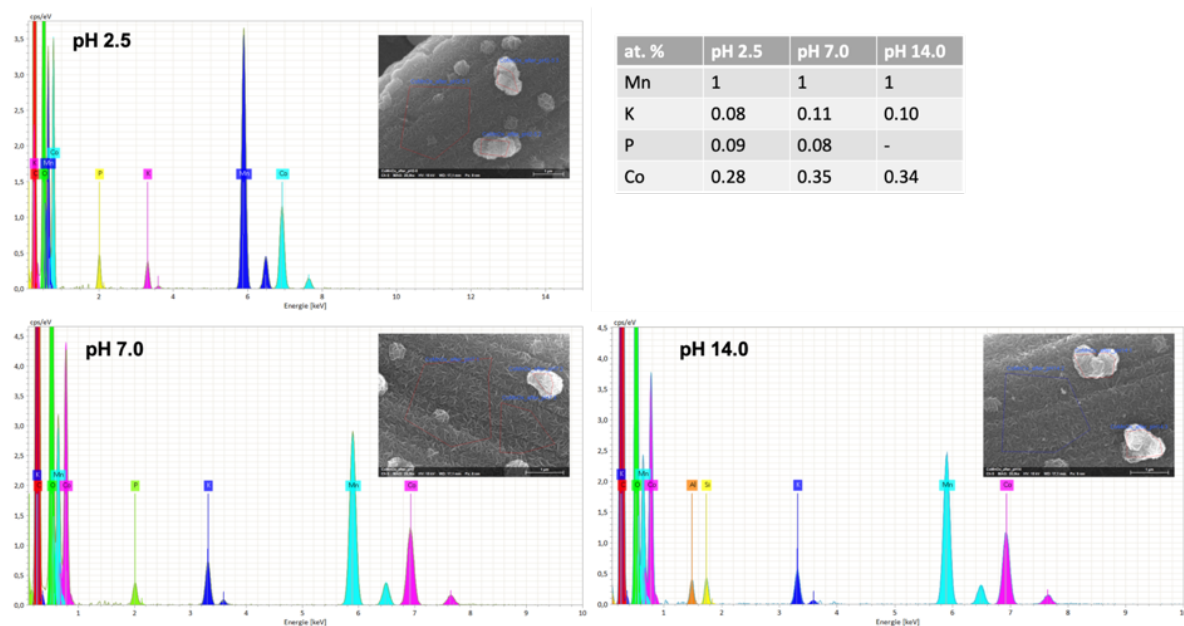| at. %	pH 2.5	pH 7.0	pH 14.0
Mn	1	1	1
K	0.10	0.12	0.06
P	0.12	0.10	-
Ni	0.09	0.09	0.11

Fig. S 13: Typical EDX spectra of $Co_{0.3}MnO_x$/CFP-electrodes after electrochemical long-term operation at pH 2.5, 7.0 and 14.0; the SEM micrograph shows the position where the EDX spectra were recorded; the table shows the molar ratios. The signal of C originates from the catalyst support.
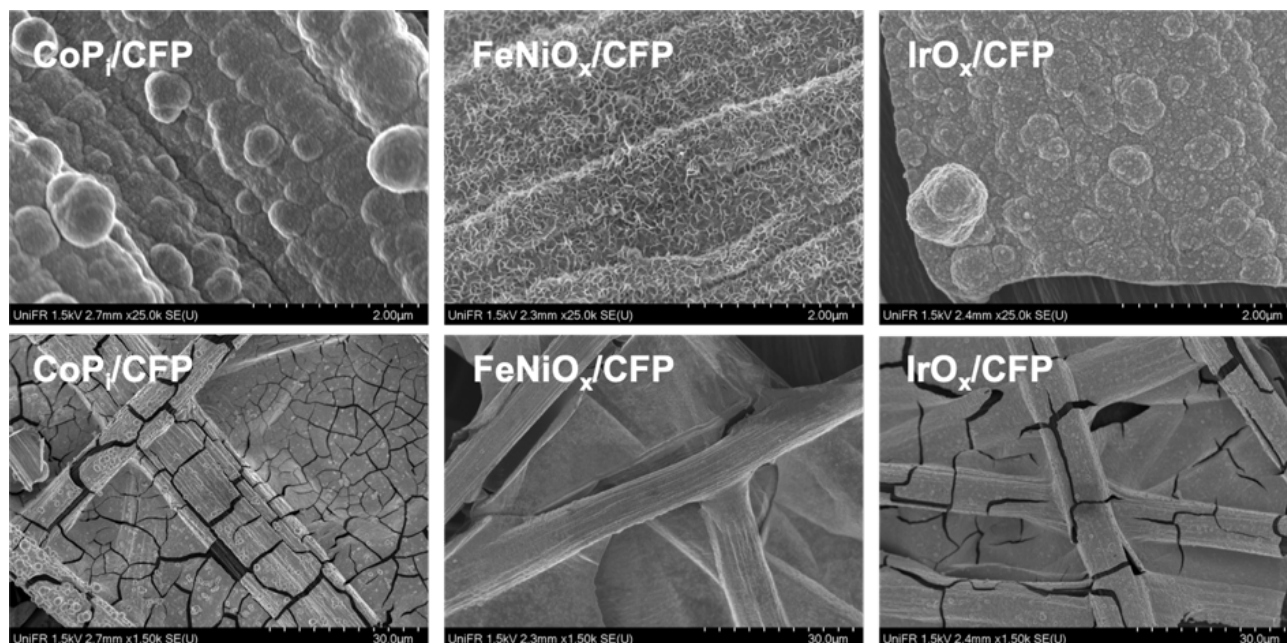

Fig. S 14: SEM micrographs at different magnifications (top row: x25k; lower row: x1.5k) of the as prepared MO_x/CFP-electrodes.
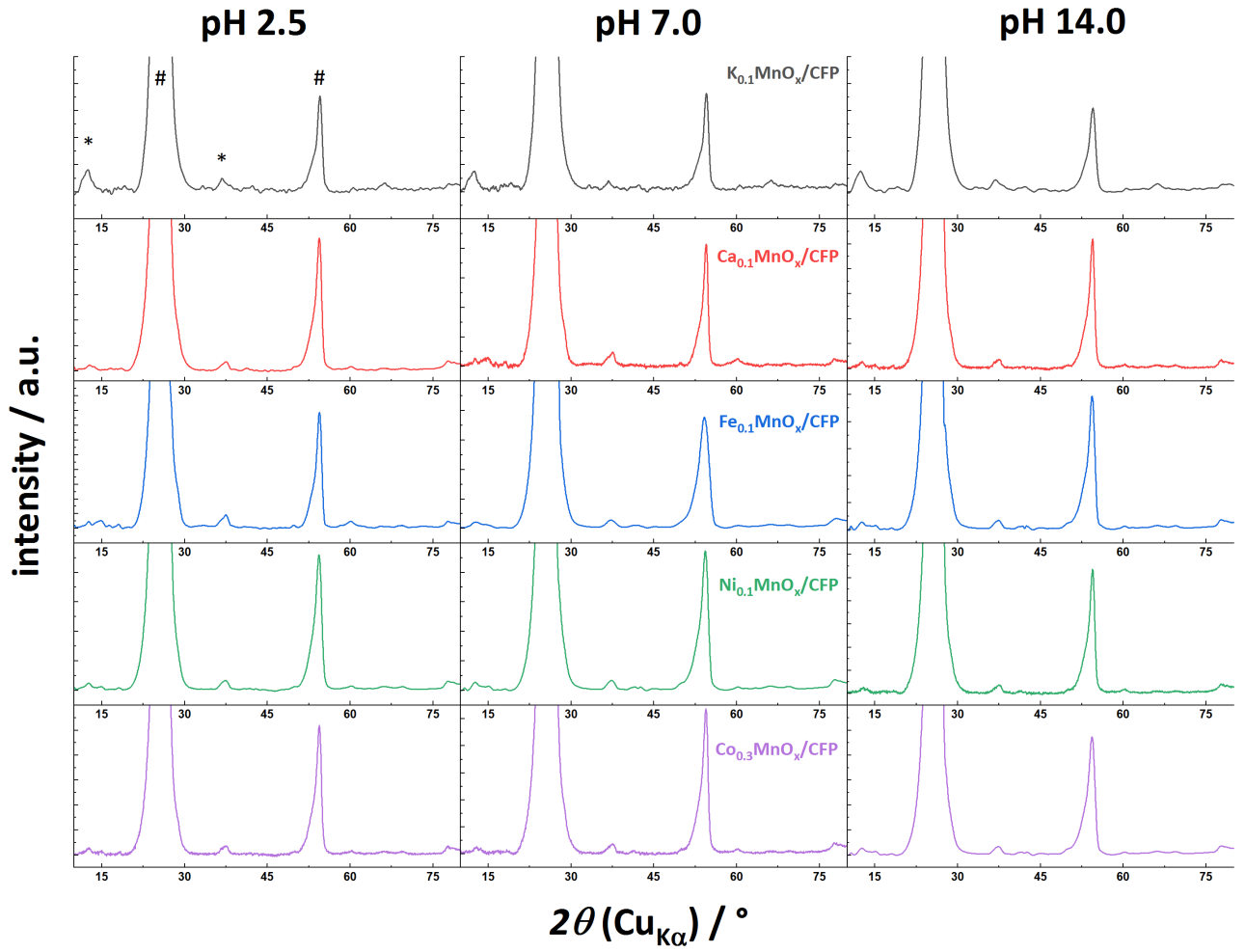
Fig. S 15: XRD patterns of $M_y MnO_x$/CFP-electrodes after operation under different pH conditions for 22 h at a constant current density $j = 2$ mA cm^{-2} (reflexes of the graphitic carbon support and the birnessite-like catalyst are labeled with $*$ and $\#$, respectively).
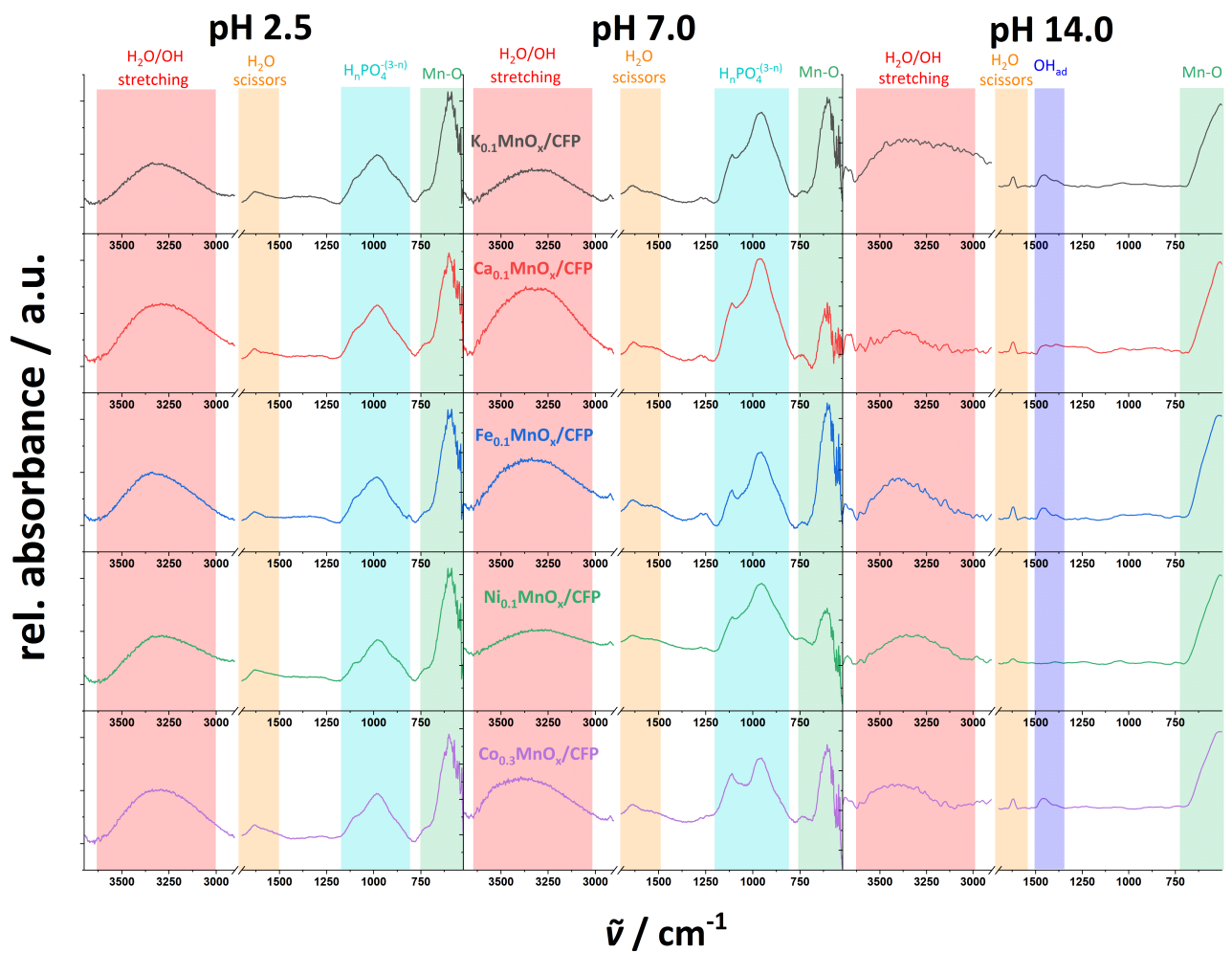
Fig. S 16: ATR-IR spectra of $M_y MnO_x$/CFP-electrodes after operation under different pH conditions for 22 h at a constant current density $j = 2$ mA cm^{-2}.
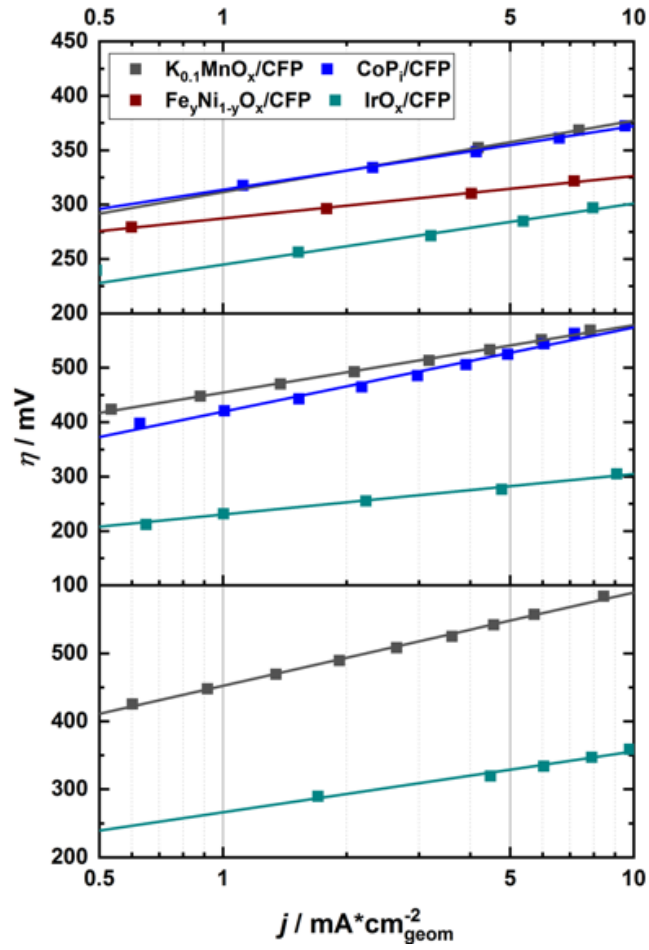
Fig. S 17: Tafel plots of MO_x/CFP-electrodes at different pH regimes and normalized to the geometric area; extracted from stepwise chronoamperometry measurements. All shown traces are the average of two individual measurements.
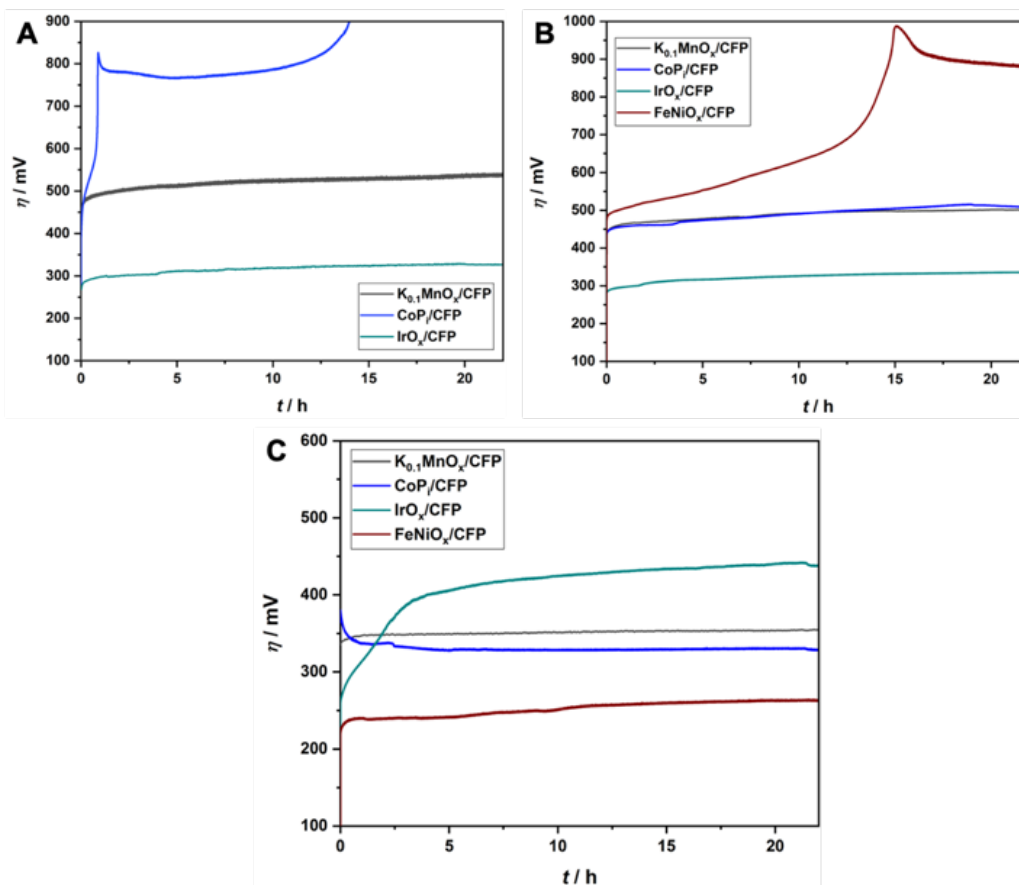
Fig. S 18: η needed to maintain a current-density of 2 mA cm^{-2} over a time of 22 h for MO$_x$/CFP-electrodes. All shown traces are the average of two individual measurements.

Tab. S 1: Nomenclature of electrodes analysed by XAS.

sample	as-prepared	after operation at pH 2.5	after operation at pH 7.0	after operation at pH 14.0
Co$_{0.3}$MnO$_x$/CFP	21	22	23	24
Ni$_{0.1}$MnO$_x$/CFP	31	32	33	34
Fe$_{0.1}$MnO$_x$/CFP	41	42	43	44
Ca$_{0.1}$MnO$_x$/CFP	51	52	53	54
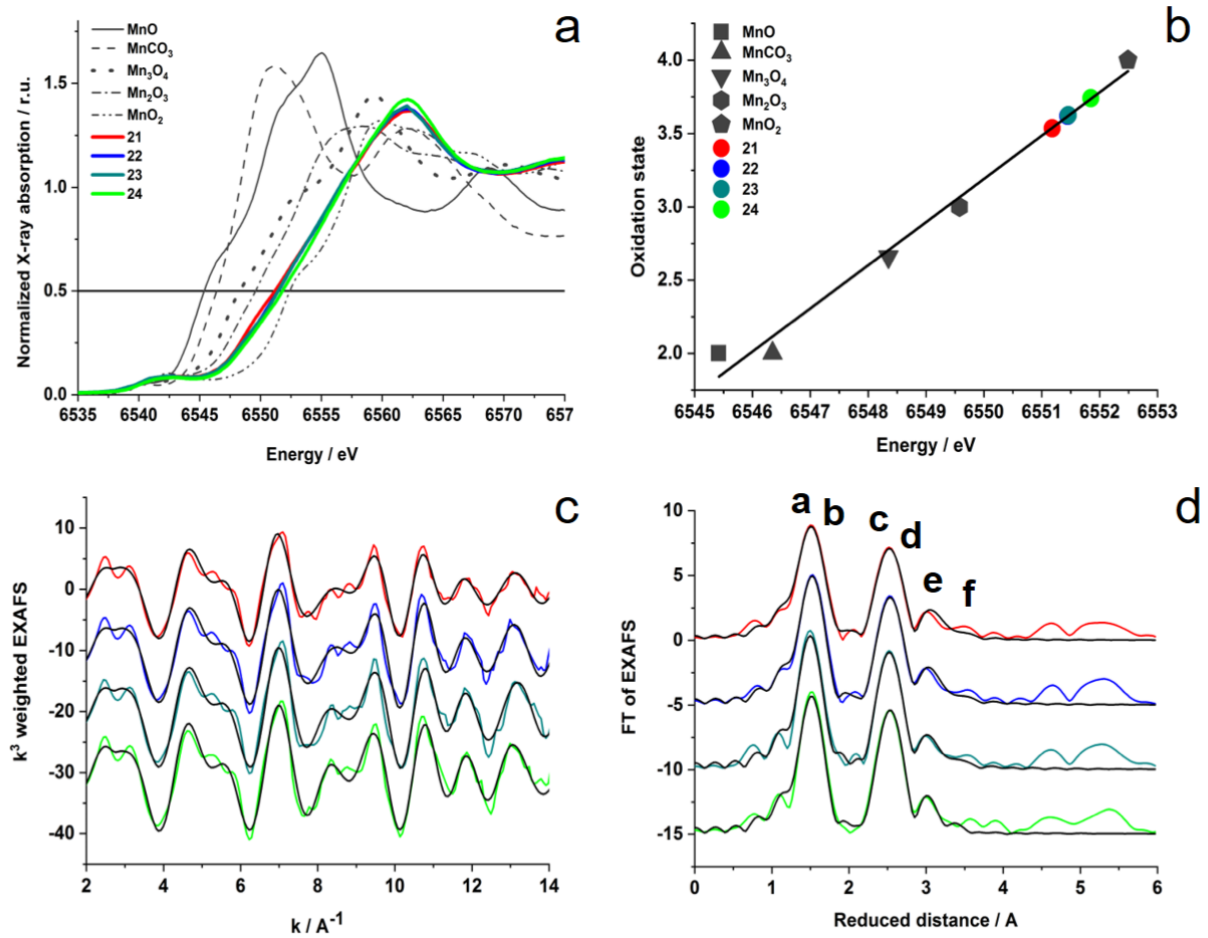
Fig. S 19: a) Mn K-edge XANES spectra of reference compounds (in grey) and deposited samples 21-24 ($Co_{0.3}MnO_x$/CFP) (in color). The horizontal line at 0.5 is used for determination of the oxidation states. b) Oxidation states of deposited samples derived from linear fit line extracted from 0.5 edge positions of reference compounds. c) k-space EXAFS spectra (k^3 weighted) and respective fits. d) Fourier transform of the EXAFS spectra (a-f denote fitted shells).
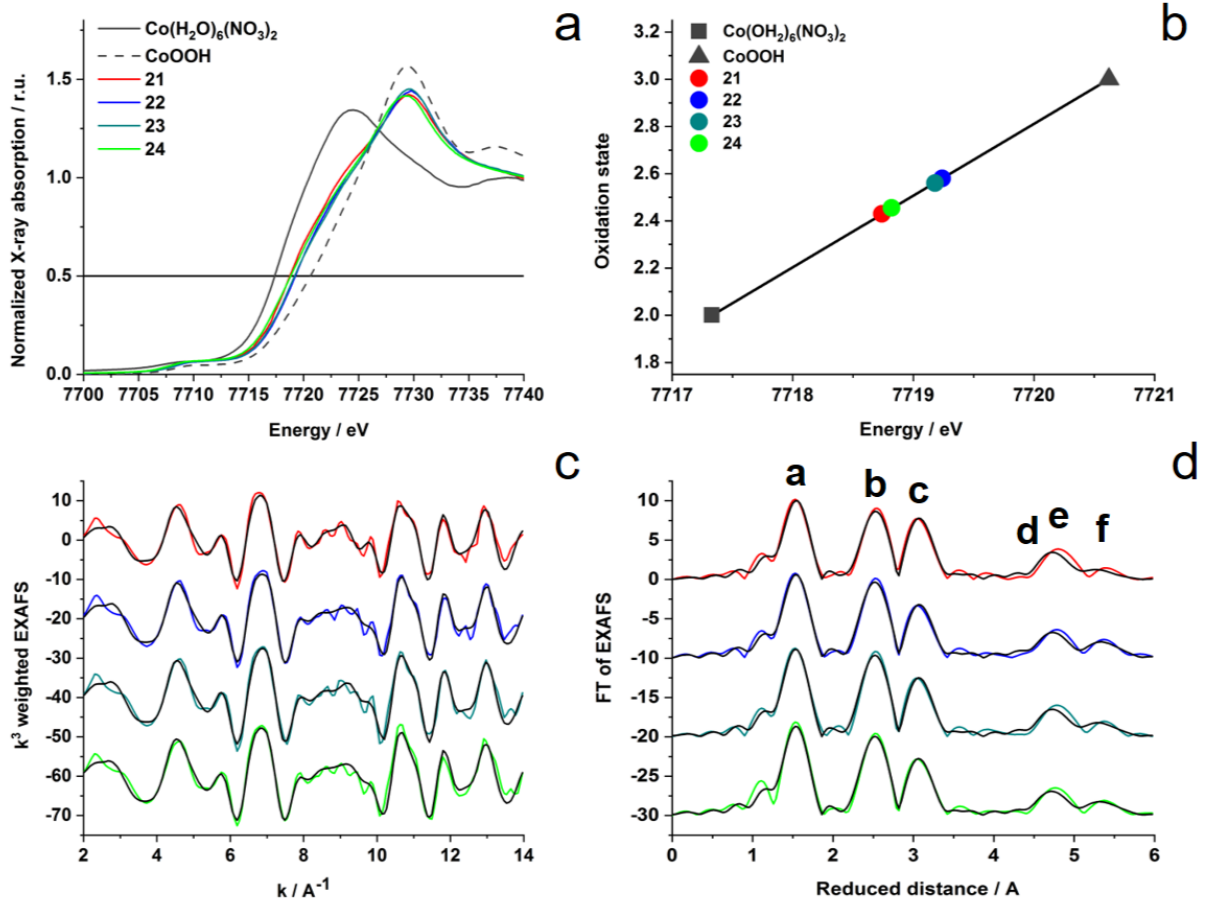
Fig. S 20: a) Co K-edge XANES spectra of reference compounds (in grey) and deposited samples 21-24 ($Co_{0.3}MnO_x$/CFP) (in color). The horizontal line at 0.5 is used for determination of the oxidation states. b) Oxidation states of deposited samples derived from linear fit line extracted from 0.5 edge positions of reference compounds. c) k-space EXAFS spectra (k^3 weighted) and respective fits. d) Fourier transform of the EXAFS spectra (a-f denote fitted shells).

Fig. S 21: a) Mn K-edge XANES spectra of reference compounds (in grey) and deposited samples 31-34 ($Ni_{0.1}MnO_x$/CFP) (in color). The horizontal line at 0.5 is used for determination of the oxidation states. b) Oxidation states of deposited samples derived from linear fit line extracted from 0.5 edge positions of reference compounds. c) k-space EXAFS spectra (k^3 weighted) and respective fits. d) Fourier transform of the EXAFS spectra (a-f denote fitted shells).
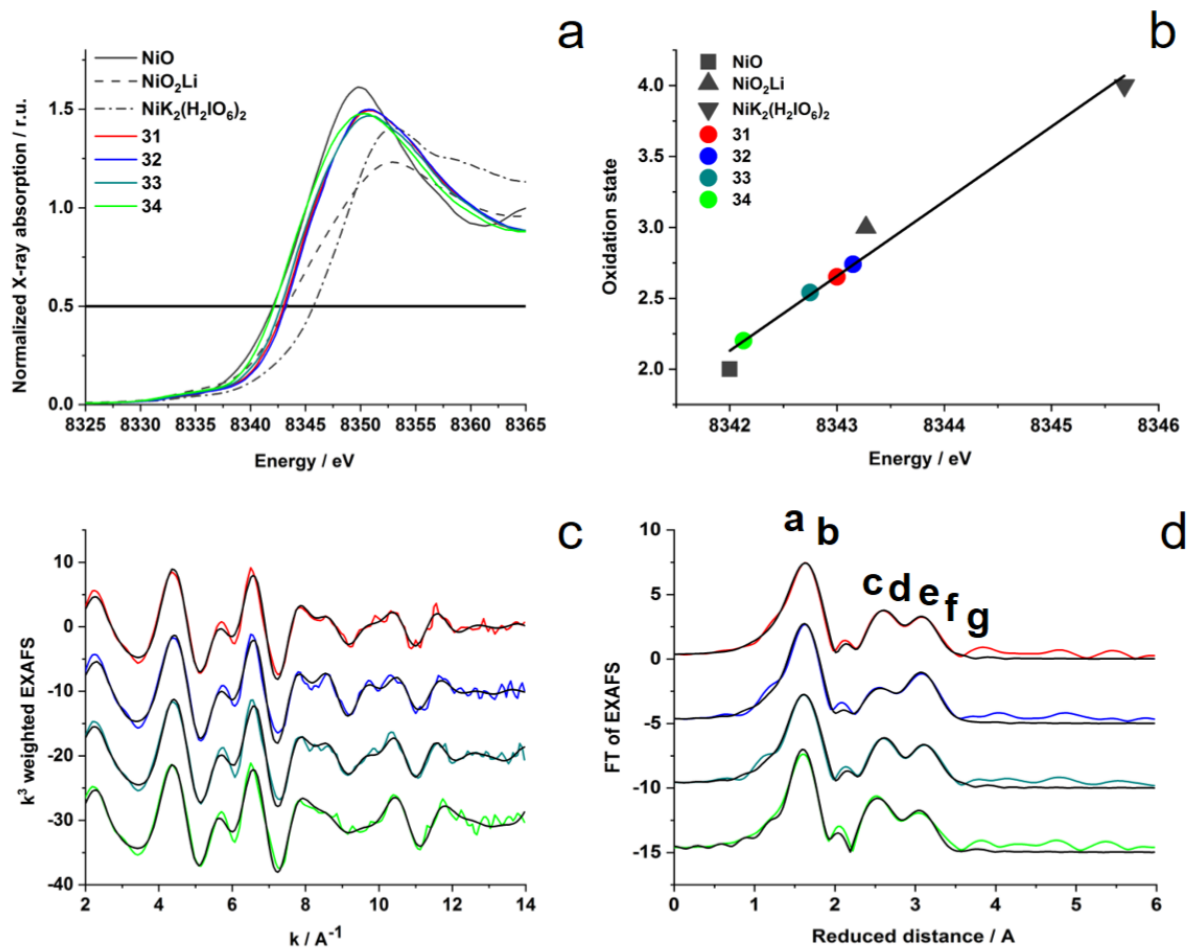
Fig. S 22: a) Ni K-edge XANES spectra of reference compounds (in grey) and deposited samples 31-34 ($Ni_{0.1}MnO_x$/CFP) (in color). The horizontal line at 0.5 is used for determination of the oxidation states. b) Oxidation states of deposited samples derived from linear fit line extracted from 0.5 edge positions of reference compounds. c) k-space EXAFS spectra (k^3 weighted) and respective fits. d) Fourier transform of the EXAFS spectra (a-f denote fitted shells).
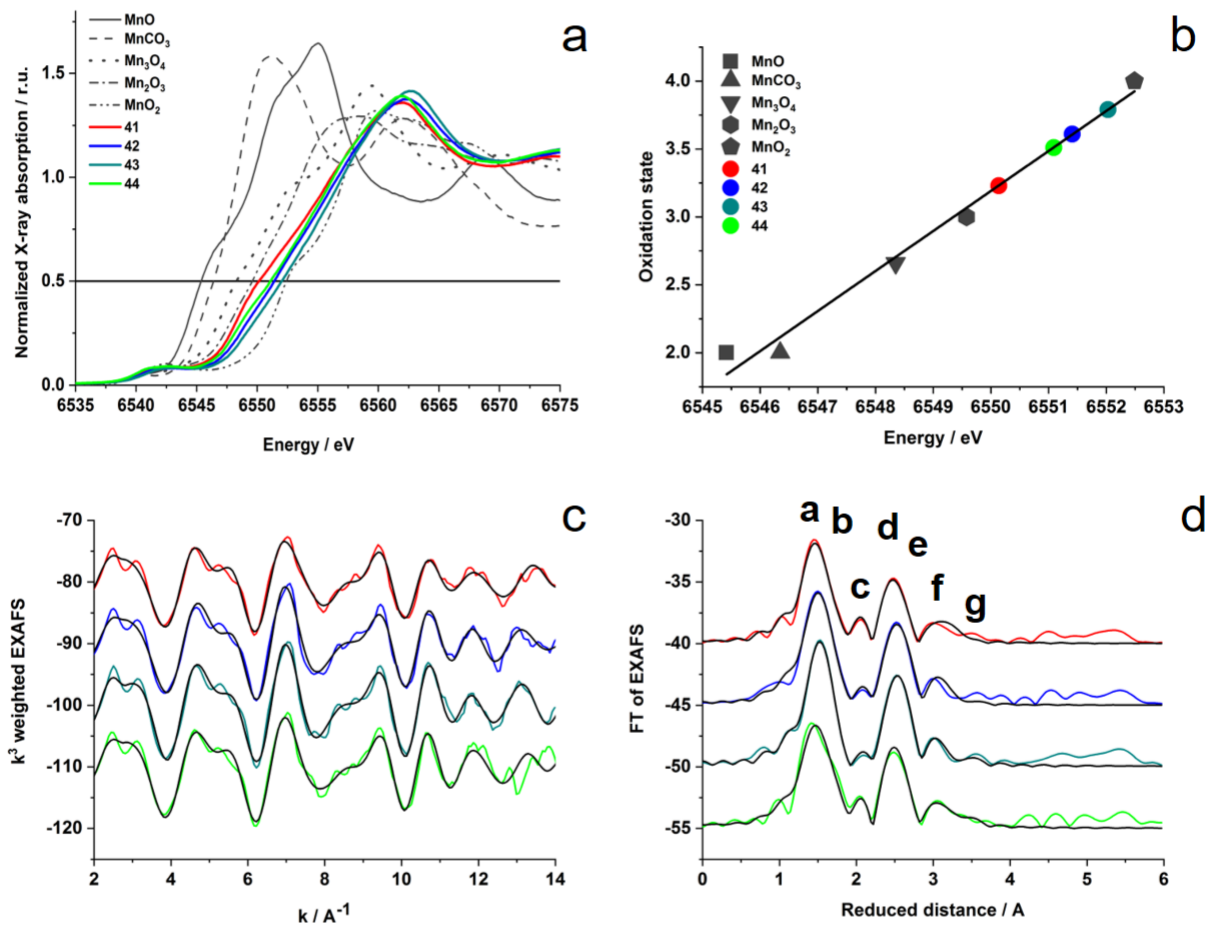
Fig. S 23: a) Mn K-edge XANES spectra of reference compounds (in grey) and deposited samples 41-44 ($Fe_{0.1}MnO_x$/CFP) (in color). The horizontal line at 0.5 is used for determination of the oxidation states. b) Oxidation states of deposited samples derived from linear fit line extracted from 0.5 edge positions of reference compounds. c) k-space EXAFS spectra (k^3 weighted) and respective fits. d) Fourier transform of the EXAFS spectra (a-g denote fitted shells).
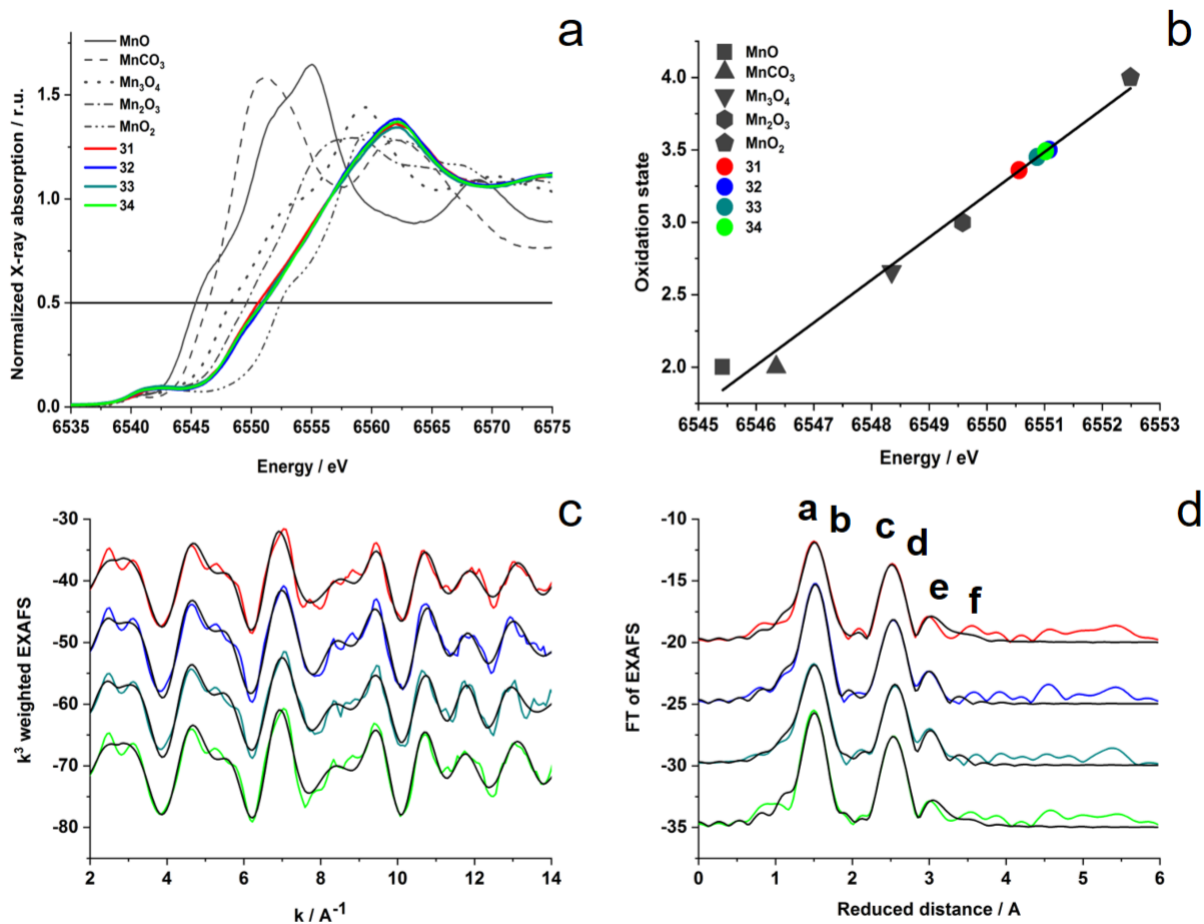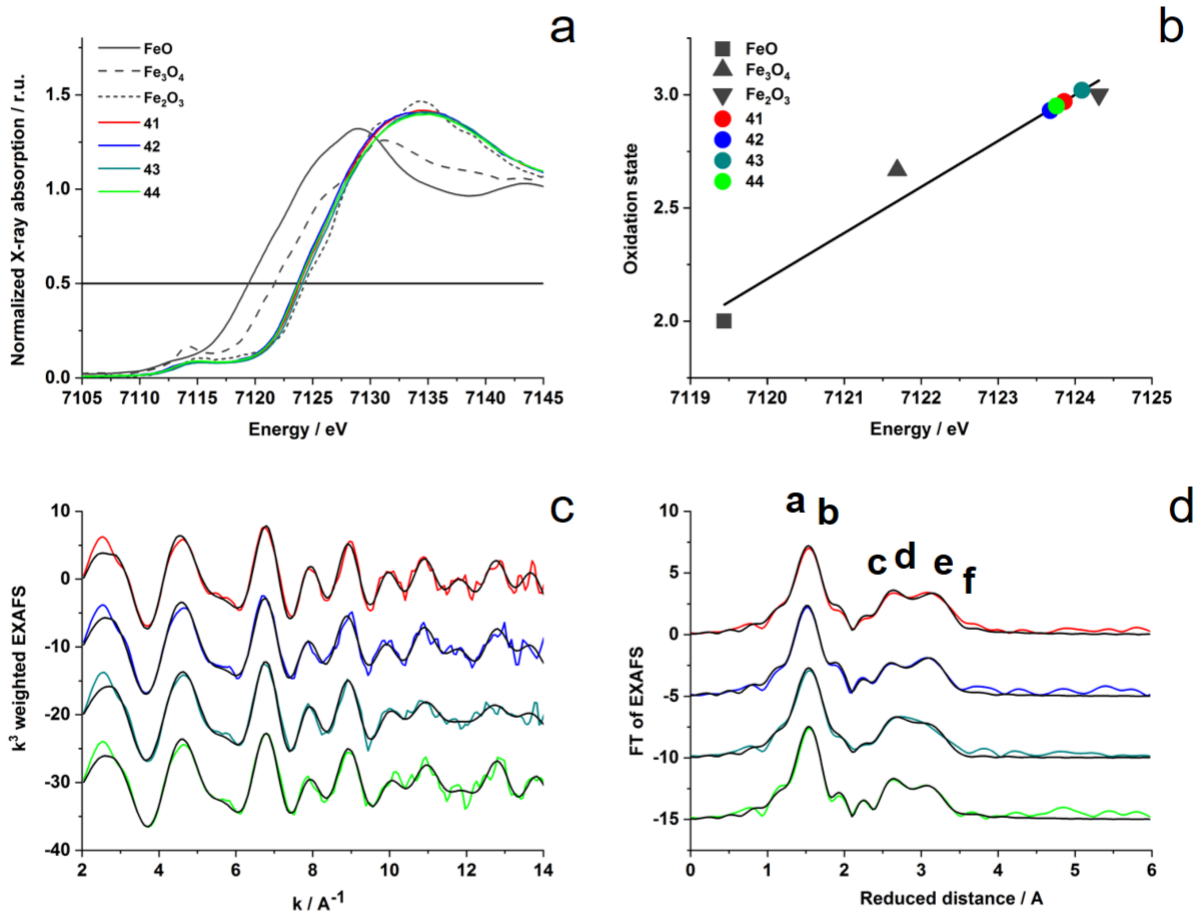
Fig. S 24: a) Fe K-edge XANES spectra of reference compounds (in grey) and deposited samples 41-44 ($Fe_{0.1}MnO_x$/CFP) (in color). The horizontal line at 0.5 is used for determination of the oxidation states. b) Oxidation states of deposited samples derived from linear fit line extracted from 0.5 edge positions of reference compounds. c) k-space EXAFS spectra (k^3 weighted) and respective fits. d) Fourier transform of the EXAFS spectra (a-f denote fitted shells).

Fig. S 25: a) Mn K-edge XANES spectra of reference compounds (in grey) and deposited samples 51-54 ($Ca_{0.1}MnO_x$/CFP) (in color). The horizontal line at 0.5 is used for determination of the oxidation states. b) Oxidation states of deposited samples derived from linear fit line extracted from 0.5 edge positions of reference compounds. c) k-space EXAFS spectra (k^3 weighted) and respective fits. d) Fourier transform of the EXAFS spectra (a-f denote fitted shells).


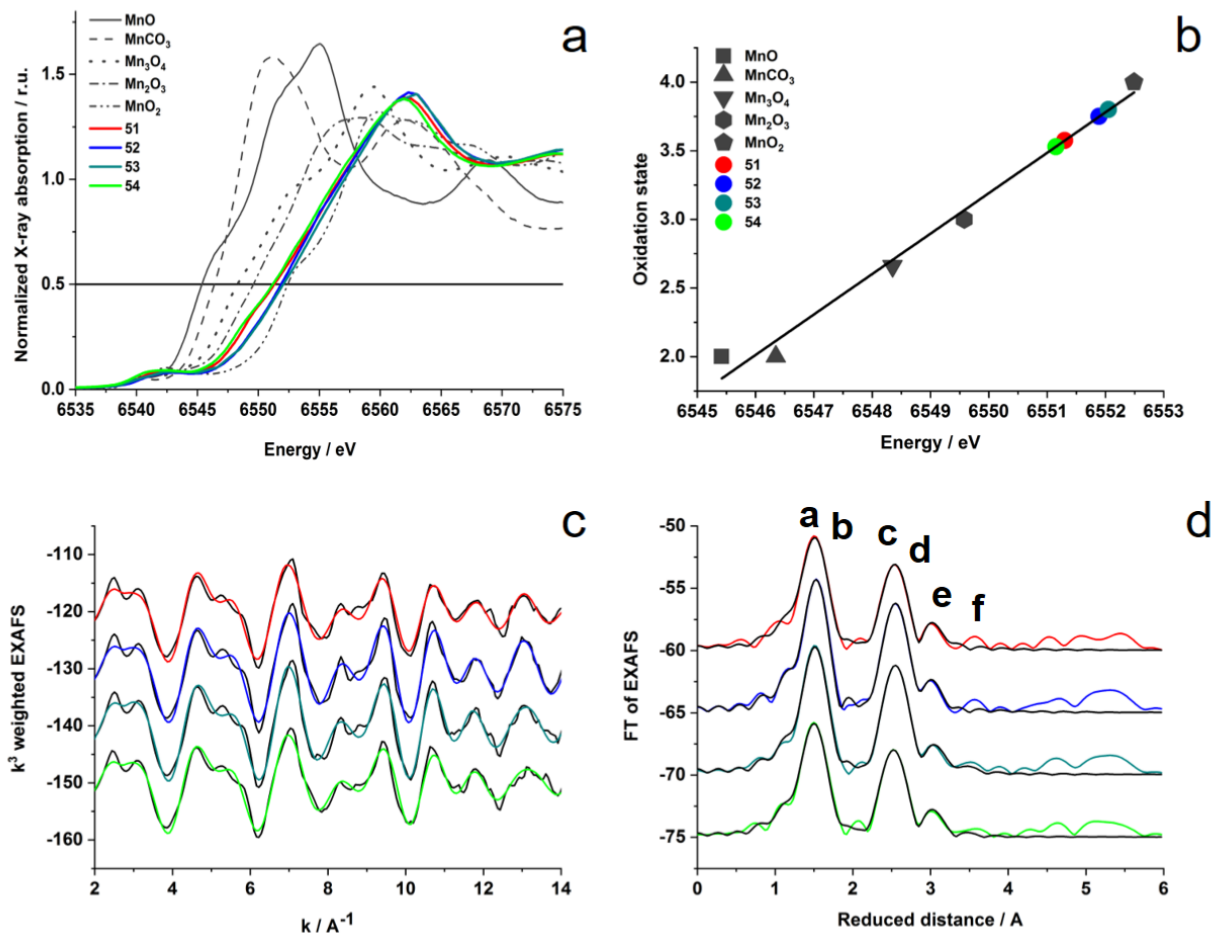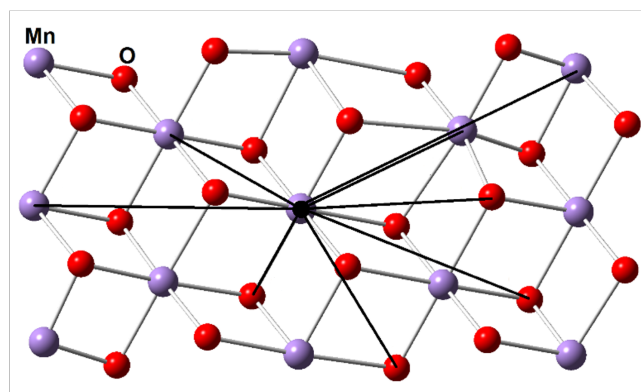**Fig. S 26:** Structural model of the deposited compounds derived from crystal structure of K-rich birnessite and artificially amorphized by small random shifts of the coordinates. Black lines denote potential scattering shells for EXAFS spectra, see Figs. S19-S25.

Tab. S 2: EXAFS fit parameters for Mn-edge of samples 21-24 (Co$_{0.3}$MnO$_x$/CFP) and 31-34 (Ni$_{0.1}$MnO$_x$/CFP).

shell	type	R [Å]	err	N	err	σ [Å]	shell	type	R [Å]	err	N	err	σ [Å]
	21		Rf			11.4		31		Rf			15.6
a	Mn-O	1.84	0.02	2.5	0.6	0.032	a	Mn-O	1.84	0.02	2.5	0.5	0.032
b	Mn-O	1.94	0.02	2.4	0.6	0.032	b	Mn-O	1.95	0.02	2.3	0.5	0.032
c	Mn-Mn	2.85	0.02	2.5	0.9	0.050	c	Mn-Mn	2.85	0.01	2.5	0.4	0.050
d	Mn-Mn	2.93	0.11	0.5	0.9	0.050	d	Mn-Mn	3.02	0.04	0.6	0.4	0.050
e	Mn-O	3.42	0.02	4.8	1.3	0.050	e	Mn-O	3.42	0.02	4.0	1.3	0.050
f	Mn-O	3.74	0.05	2.0	1.7	0.050	f	Mn-O	3.79	0.06	2.0	1.7	0.050
	22		Rf			11.7		32		Rf			13.3
a	Mn-O	1.84	0.03	2.4	1.00	0.032	a	Mn-O	1.84	0.02	2.6	0.8	0.032
b	Mn-O	1.93	0.03	2.6	1.00	0.032	b	Mn-O	1.94	0.02	2.5	0.8	0.032
c	Mn-Mn	2.85	0.01	3.0	0.3	0.050	c	Mn-Mn	2.79	0.16	0.6	2.4	0.050
d	Mn-Mn	3.09	0.12	0.2	0.4	0.050	d	Mn-Mn	2.86	0.05	2.1	2.4	0.050
e	Mn-O	3.41	0.02	5.3	1.3	0.050	e	Mn-O	3.41	0.02	5.7	1.4	0.050
f	Mn-O	3.72	0.04	2.5	1.6	0.050	f	Mn-O	3.59	0.05	2.2	1.6	0.050
	23		Rf			15.4		33		Rf			14.7
a	Mn-O	1.86	0.01	3.7	0.5	0.032	a	Mn-O	1.83	0.02	2.5	0.5	0.032
b	Mn-O	1.97	0.03	1.7	0.5	0.032	b	Mn-O	1.95	0.02	2.4	0.5	0.032
c	Mn-Mn	2.84	0.01	3.4	0.4	0.050	c	Mn-Mn	2.70	0.05	0.4	0.3	0.050
d	Mn-Mn	3.01	0.07	0.3	0.4	0.050	d	Mn-Mn	2.86	0.01	2.6	0.4	0.050
e	Mn-O	3.41	0.02	5.1	1.4	0.050	e	Mn-O	3.42	0.02	6.1	1.4	0.050
f	Mn-O	3.68	0.04	2.8	1.7	0.050	f	Mn-O	3.62	0.04	2.5	1.8	0.050
	24		Rf			15.0		34		Rf			16.5
a	Mn-O	1.86	0.02	3.3	0.8	0.032	a	Mn-O	1.86	0.01	3.2	0.5	0.032
b	Mn-O	1.96	0.03	2.1	0.8	0.032	b	Mn-O	1.97	0.03	1.8	0.5	0.032
c	Mn-Mn	2.84	0.03	3.3	1.9	0.050	c	Mn-Mn	2.86	0.01	2.8	0.4	0.050
d	Mn-Mn	2.91	0.18	0.5	1.8	0.050	d	Mn-Mn	2.99	0.10	0.3	0.4	0.050
e	Mn-O	3.41	0.02	5.8	1.4	0.050	e	Mn-O	3.42	0.02	4.4	1.3	0.050
f	Mn-O	3.63	0.04	2.5	1.8	0.050	f	Mn-O	3.76	0.05	2.0	1.7	0.050

The range of the fits was 2-14 Å^{-1}. R is the absorber-backscatter distance, N the EXAFS coordination number, σ the Debye Waller factor. The Rf value was calculated between 1 and 4 Å reduced distance and provides the fit quality in percent. The amplitude reduction factor, $S_0^2(k)$, was 0.70 in all refinements. The errors represent the 68% confidence interval of the respective fit parameter. Please note: The assigned Co/Ni/Fe/Mn-Mn shells are most likely not pure metal-to-manganese shells, but contain contributions of both involved metal types. Metal backscatter was assigned to be Mn in all cases due to stochiometric considerations.

Tab. S 3: EXAFS fit parameters for Mn-edge of samples 41-44 ($Fe_{0.1}MnO_x$/CFP) and 51-54 ($K_{0.1}MnO_x$/CFP).

shell	type	R [Å]	err	N	err	σ [Å]	shell	type	R [Å]	err	N	err	σ [Å]
	41		Rf			13.8		51		Rf			13.5
a	Mn-O	1.84	0.01	3.3	0.4	0.032	a	Mn-O	1.84	0.02	2.7	0.6	0.032
b	Mn-O	1.98	0.02	2.4	0.4	0.032	b	Mn-O	1.95	0.02	2.5	0.6	0.032
c	Mn-O	2.24	0.02	1.3	0.5	0.032							
d	Mn-Mn	2.84	0.01	2.0	0.4	0.050	c	Mn-Mn	2.80	0.12	0.8	2.1	0.050
e	Mn-Mn	2.99	0.05	0.6	0.4	0.050	d	Mn-Mn	2.87	0.05	2.1	2.1	0.050
f	Mn-O	3.44	0.02	4.7	1.3	0.050	e	Mn-O	3.40	0.05	4.1	2.4	0.050
g	Mn-O	3.76	0.08	1.3	1.7	0.050	f	Mn-O	3.52	0.08	2.8	2.3	0.050
	42		Rf			14.7		52		Rf			9.1
a	Mn-O	1.84	0.02	2.9	0.5	0.032	a	Mn-O	1.83	0.03	2.0	1.1	0.032
b	Mn-O	1.95	0.02	2.7	0.5	0.032	b	Mn-O	1.92	0.02	3.1	1.1	0.032
c	Mn-O	2.27	0.03	0.8	0.4	0.032							
d	Mn-Mn	2.82	0.13	1.2	4.7	0.050	c	Mn-Mn	2.71	0.10	0.2	0.3	0.050
e	Mn-Mn	2.88	0.10	1.5	4.7	0.050	d	Mn-Mn	2.88	0.03	2.9	1.6	0.050
f	Mn-O	3.41	0.02	4.4	1.3	0.050	e	Mn-O	3.44	0.02	5.3	1.5	0.050
g	Mn-O	3.76	0.08	1.3	1.7	0.050	f	Mn-O	3.60	0.10	1.4	1.7	0.050
	43		Rf			8.2		53		Rf			10.7
a	Mn-O	1.85	0.02	2.9	0.9	0.032	a	Mn-O	1.84	0.02	3.1	0.7	0.032
b	Mn-O	1.95	0.03	2.6	0.8	0.032	b	Mn-O	1.95	0.02	2.4	0.7	0.032
c	Mn-O	2.28	0.04	0.7	0.4	0.032							
d	Mn-Mn	2.85	0.02	2.6	0.5	0.050	c	Mn-Mn	2.80	0.08	0.9	1.6	0.050
e	Mn-Mn	2.97	0.18	0.2	0.5	0.050	d	Mn-Mn	2.88	0.03	2.9	1.6	0.050
f	Mn-O	3.43	0.02	7.0	1.8	0.071	e	Mn-O	3.45	0.02	5.6	1.4	0.050
g	Mn-O	3.71	0.05	3.5	2.3	0.071	f	Mn-O	3.69	0.04	2.4	1.7	0.050
	44		Rf			14.0		54		Rf			13.4
a	Mn-O	1.83	0.01	3.1	0.4	0.032	a	Mn-O	1.84	0.02	2.8	0.6	0.032
b	Mn-O	1.96	0.02	3.0	0.4	0.032	b	Mn-O	1.95	0.02	2.3	0.6	0.032
c	Mn-O	2.25	0.02	1.3	0.5	0.032							
d	Mn-Mn	2.86	0.01	2.6	0.4	0.050	c	Mn-Mn	2.84	0.03	2.3	1.1	0.050
e	Mn-Mn	3.03	0.05	0.6	0.5	0.050	d	Mn-Mn	2.92	0.08	0.8	1.1	0.050
f	Mn-O	3.44	0.02	4.9	1.4	0.050	e	Mn-O	3.44	0.02	5.4	1.5	0.050
g	Mn-O	3.75	0.06	2.2	1.7	0.050	f	Mn-O	3.63	0.06	1.7	1.8	0.050

The range of the fits was 2-14 Å^{-1}. R is the absorber-backscatter distance, N the EXAFS coordination number, $σ$ the Debye Waller factor. The Rf value was calculated between 1 and 4 Å reduced distance and provides the fit quality in percent. The amplitude reduction factor, $S_0^2(k)$, was 0.70 in all refinements. The errors represent the 68% confidence interval of the respective fit parameter. Please note: The assigned Co/Ni/Fe/Mn-Mn shells are most likely not pure metal-to-manganese shells, but contain contributions of both involved metal types. Metal backscatter was assigned to be Mn in all cases due to stochiometric considerations.

Tab. S 4: EXAFS fit parameters for the Co, Fe, and Ni-edges of samples 21-24 ($Co_{0.3}MnO_x$/CFP), 31-34 (Ni0.1MnOx/CFP), and 41-44 ($Fe_{0.1}MnO_x$/CFP).

shell	type	R [Å]	err	N	err	shell	type	R [Å]	err	N	err	shell	type	R [Å]	err	N	err
	21		Rf	15.9			31		Rf	9.5			41		Rf	16.4	
a	Co-O	1.91	0.01	4.2	0.3	a	Ni-O	1.93	0.02	2.1	0.4	a	Fe-O	1.91	0.01	3.4	0.3
b	Co-Mn	2.85	0.01	2.7	0.2	b	Ni-O	2.05	0.02	3.1	0.4	b	Fe-O	2.06	0.01	2.2	0.3
c	Co-Mn	3.37	0.01	3.5	0.3	c	Ni-Mn	2.83	0.05	0.5	0.4	c	Fe-Mn	2.83	0.02	1.0	0.3
d	Co-O	4.79	0.05	5.7	4.0	d	Ni-Mn	2.94	0.03	1.0	0.3	d	Fe-Mn	2.98	0.01	1.9	0.3
e	Co-Mn	4.99	0.01	5.7	1.2	e	Ni-O	3.35	0.03	5.6	1.4						
f	Co-Mn	5.44	0.12	1.1	1.7	f	Ni-Mn	3.49	0.04	1.0	0.5	e	Fe-Mn	3.40	0.01	1.9	0.3
g	MS(b,f)	2.78	0.02	1.1		g	Ni-O	3.75	0.07	1.4	1.5	f	Fe-O	3.64	0.02	3.9	1.2
	22		Rf	13.4			32		Rf	11.5			42		Rf	13.5	
a	Co-O	1.90	0.01	4.4	0.3	a	Ni-O	1.95	0.02	2.5	0.5	a	Fe-O	1.90	0.01	3.6	0.2
b	Co-Mn	2.84	0.01	3.1	0.2	b	Ni-O	2.06	0.02	2.6	0.5	b	Fe-O	2.06	0.01	2.3	0.3
c	Co-Mn	3.37	0.01	2.9	0.3	c	Ni-Mn	2.84	0.03	0.7	0.3	c	Fe-Mn	2.83	0.02	0.7	0.3
d	Co-O	4.79	0.04	6.5	3.9	d	Ni-Mn	2.97	0.04	0.7	0.3	d	Fe-Mn	2.98	0.01	1.4	0.3
e	Co-Mn	4.98	0.01	5.4	1.1	e	Ni-O	3.34	0.03	5.2	1.4						
f	Co-Mn	5.47	0.06	3.1	1.8	f	Ni-Mn	3.47	0.02	1.3	0.6	e	Fe-Mn	3.40	0.01	1.8	0.3
g	MS(b,f)	2.77	0.02	3.1		g	Ni-O	3.78	0.05	1.4	1.3	f	Fe-O	3.63	0.04	2.0	1.2
	23		Rf	15.3			33		Rf	13.0			43		Rf	14.0	
a	Co-O	1.90	0.01	4.6	0.3	a	Ni-O	1.94	0.02	2.2	0.5	a	Fe-O	1.90	0.01	3.3	0.3
b	Co-Mn	2.84	0.01	3.3	0.2	b	Ni-O	2.05	0.02	2.8	0.5	b	Fe-O	2.04	0.02	2.1	0.3
c	Co-Mn	3.37	0.01	3.2	0.3	c	Ni-Mn	2.77	0.06	0.3	0.2	c	Fe-Mn	2.83	0.02	0.7	0.3
d	Co-O	4.79	0.05	6.0	3.9	d	Ni-Mn	2.91	0.02	1.2	0.2	d	Fe-Mn	2.98	0.01	1.7	0.3
e	Co-Mn	4.98	0.01	5.8	1.1	e	Ni-O	3.33	0.02	6.0	1.4						
f	Co-Mn	5.44	0.08	1.9	1.8	f	Ni-Mn	3.49	0.03	1.7	0.6	e	Fe-Mn	3.38	0.01	1.4	0.3
g	MS(b,f)	2.77	0.02	1.9		g	Ni-O	3.72	0.04	2.5	1.8	f	Fe-O	3.70	0.05	1.4	1.1
	24		Rf	17.6			34		Rf	11.6			44		Rf	8.2	
a	Co-O	1.90	0.01	4.8	0.3	a	Ni-O	1.98	0.01	3.6	0.3	a	Fe-O	1.91	0.01	3.5	0.3
b	Co-Mn	2.84	0.01	3.2	0.2	b	Ni-O	2.12	0.03	1.4	0.3	b	Fe-O	2.06	0.02	1.7	0.3
c	Co-Mn	3.37	0.01	3.1	0.3	c	Ni-Mn	2.88	0.01	1.6	0.4	c	Fe-Mn	2.79	0.03	0.5	0.2
d	Co-O	4.79	0.06	4.8	3.9	d	Ni-Mn	3.03	0.04	1.0	0.7	d	Fe-Mn	2.96	0.01	1.5	0.3
e	Co-Mn	4.98	0.01	5.0	1.1	e	Ni-O	3.29	0.08	5.0	1.9						
f	Co-Mn	5.47	0.07	2.7	1.8	f	Ni-Mn	3.46	0.06	2.4	1.2	e	Fe-Mn	3.39	0.01	1.8	0.4
g	MS(b,f)	2.77	0.03	2.7		g	Ni-O	3.58	0.10	3.6	3.7	f	Fe-O	3.58	0.04	2.2	1.4

The range of the fits was 2-14 Å^{-1}. R is the absorber-backscatter distance and N the EXAFS coordination number. The Rf value was calculated between 1 and 6 Å(Co) or 1 and 4 Å(Ni, Fe) reduced distance and provides the fit quality in percent. The Debye Waller parameter, σ, was set to 0.05 for all shells in all fits. The amplitude reduction factor, $S_0^2(k)$, was 0.80 (Co), 0.90 (Ni), and 0.75 (Fe) in all refinements. The errors represent the 68% confidence interval of the respective fit parameter. MS(b,f) refers to a multiple-scattering shell involving shells b at about 2.8 Åand shell f at roughly the double-distance of about 5.5 Å. Please note: The assigned Co/Ni/Fe/Mn-Mn shells are most likely not pure metal-to-manganese shells, but contain contributions of both involved metal types. Metal backscatter was assigned to be Mn in all cases due to stochiometric considerations.

References

[1] A. L. Ankudinov, B Ravel, J. J. Rehr, S. D. Conradson, *Phys. Rev. B* **1998**, *58*, 7565–7576.